Int. J. Electrochem. Sci., 15 **(2020)** 5540 – 5551, doi: 10.20964/2020.06.51

International Journal of
ELECTROCHEMICAL
SCIENCE
www.electrochemsci.org

Efficient Solar Cells Constructed with Lead Iodide Perovskite Templated by a 3-aminopropyl trimethoxysilane and methyltrimethoxysilane Mixed Monolayer

Qinghua Liu[1,2,*], *Dianlu Jiang*[3,**], *Qing Kang*[4], *Feimeng Zhou*[3,***]

[1] College of Chemistry and Chemical Engineering, Central South University, Changsha, Hunan 410083, P.R. China
[2] School of Chemistry and Chemical Engineering, Heze University, Heze 274015, China
[3] Department of Chemistry and Biochemistry, California State University, Los Angeles, Los Angeles, California 90032
[4] Institute of Surface Analysis and Chemical Biology, University of Jinan, Jinan, Shandong 250022, P. R. China
[*]E-mail: liuqinghua-126@126.com;
[**]E-mail: djiang4@calstatela.edu
[***]E-mail: fzhou@calstatela.edu

Received: 24 January 2020 / *Accepted:* 16 March 2020 / *Published:* 10 May 2020

A lead iodide perovskite solar cell has been designed using a mixed monolayer of (3-aminopropyl)trimethoxysilane (APS) and methyltrimethoxysilane (MTMS) self-assembled on a compact TiO_2 layer to template the perovskite film growth. The dispersed aminopropyl groups at the surface, upon conversion to $(CH_2)_3NH_3^+I^-$, form the bottommost layer of the perovskite film. The effect of the APS/MTMS compositions in the mixed monolayers on the performance of the perovskite solar cells (PSCs) was investigated by measuring the power conversion efficiency. We developed a surface modification procedure with which the [APS]/[MTMS] ratios in solution match exactly the compositions of APS and MTMS in the resultant mixed monolayers. At the [APS]/[MTMS] ratio of 50/50, the distance between two adjacent Si atoms matches well with the lattice constant of the lead iodide perovskite crystal, and the power conversion efficiency of PSCs increases from 13.2% (without the monolayer) to 17.5%. X-ray diffraction patterns suggest that the templated perovskite growth is along the (110) plane, with enhanced orientation and crystallinity. The increase in electron lifetime of the solar cell indicates that the number of photohole/electron recombination sites is reduced and charge transport at the perovskite film/TiO_2 interface is facilitated.

Keywords: Mixed organosilane monolayer, Covalent anchor, Orientation, template, Lead iodide perovskite

1. INTRODUCTION

Organic lead halide perovskites have been widely used as light harvesters for the third-generation photovoltaic solar cells, owing to desirable properties such as high absorption coefficients [1, 2], appropriate band gaps [3, 4], long carrier diffusion lengths [5, 6], and high charge carrier mobility [7]. Significant progress has been made in designing various devices, which include the classic mesoporous-free planar configurations and mesoporous-infiltrated n-i-p and p-i-n junctions [8, 9]. In less than a decade, the power conversion efficiency of perovskite solar cells (PSCs) has been rapidly improved from 3.8% in 2009 to 24.2% in 2019 [10].

Interfaces between different layers of solar cells are critical to the photovoltaic performance (i.e. power conversion efficiency). An optimal solar cell requires an interface that is free of recombination channels or sites and imposes a small energy barrier to charge transport. A proper surface modification of the TiO_2 layer in dye-sensitized solar cells (DSSCs) can accelerate the hole/electron separation, thereby avoiding the detrimental hole/electron recombination [11]. For example, bis-2,2′-bipyridine-4-carboxylic acid was used to anchor organic dye molecules to TiO_2 and improved the DSSC efficiency [12]. Our earlier work has shown that organosilane passivation of an array of TiO_2 nanowires can effectively block channels accessible to the redox couple in solution, while hindering the recombination between photogenerated holes and electrons [13]. Similar strategies have also been used to construct PSCs to immobilize $CH_3NH_3PbI_3$ onto TiO_2 [14]. Ogomi et al. explored the use of a monolayer of $HOCO–R–NH_3^+I^-$ (R is an alkyl chain), covalently attached to TiO_2, as a template to modulate the orientation of perovskite crystals [15]. With amino acids as the anchors to grow the perovskite, Shih et al. attained a 12.02% conversion efficiency, a sizable improvement over that of the unmodified (8.35%) [16]. In addition to amino acids [16-18] and silanes [14, 19], $TiCl_4$ [20] and thiols [21] have been utilized to modify the TiO_2 layer for facilitating charge transport and minimizing charge recombination.

The uniform coverage and spacing of the functional groups in the modifying monolayer exert significant impacts on the property of the interface. Steric hindrance imposed by densely populated amino groups can prevent perovskite films from growing orderly at the modified TiO_2/perovskite interface. To our knowledge, no systematic studies have been carried out to correlate the structure of the anchor monolayer (e.g. the use of mixed monolayer and different alkyl chains to pattern the surface) to the quality of the perovskite, which governs the ultimate PSC performance.

Organosilanes such as 3-aminopropyl trimethoxysilane (APS) and methyltrimethoxysilane (MTMS) have been widely used to produce single- and multi-layered films at different surfaces [22], including TiO_2 nanoparticles and nanowires [13-15]. As a wide range of organosilane molecules are commercially available [23], many mixed organosilane monolayers of varying surface compositions can be produced. However, a mixed monolayer of two organosilane molecules constructed at the compact TiO_2 layer and its subsequent use as an anchor layer for the perovskite growth have not reported. If the density and functionality of the tether groups are favorable to oriented growth of the perovskite crystal, high-performance PSCs can be constructed. Inspired by the use of mixed alkanethiol monolayers comprising two different alkyl chain lengths to immobilize biomolecules with reduced steric hindrance [24-26], we could fabricate a mixed monolayer of APS and MTMS wherein the protruding $(CH_2)_3NH_2$, upon conversion to $(CH_2)_3NH_3^+I^-$, serve as anchors for the growth of perovskite. In addition, if we adjust

the ratio of APS and MTMS so that the distance between two adjacent $(CH_2)_3NH_3^+$ groups matches the lattice constant of $CH_3NH_3PbI_3$ crystal, the perovskite composition could possess the highest crystallinity and the best orientation. The forming perovskite with such a mixed monolayer will simultaneously minimize the energy barrier at the TiO_2/perovskite interface to the charge transport.

2. EXPERIMENTAL SECTION

2.1. Chemicals and materials.

Fluorine-doped tin oxide (FTO) glasses (Tec 15, 10 Ω/square) were purchased from Hartford Glass (Hartford, IN, USA). Lead iodide (PbI_2, 99.999%) was acquired from Strem Chemical (Newburyport, MA, USA). Zinc powder (99.995%), HCl (37%), HI (57%), methylammonium iodide (CH_3NH_3I, 98%), 4-tert-butylpyridine (TBP, 96%), tris(2-(1H-pyrazol-1-yl)-4-tert-butylpyridine)cobalt(II) di[bis(trifluoromethane)sulfo-namide] (Co-TFSI, 98%) and 2,2,7,7-tetrakis-(*N*,*N*-di-p-methoxyphenylamine)-9,9-spirobifluorene (spiro-OMeTAD, 99%) were obtained from Sigma Aldrich (St. Louis, MO, USA). Isopropanol (99.8%), ethanolamine (>99.5%), toluene (99.85%), chlorobenzene (99.8%), tetrabutyl titanate (99%), *N*, *N*-dimethylformamide (99.8%), (3-aminopropyl)trimethoxysilane (APS, 98%), methyltrimethoxysilane (MTMS, 97%) and lithium-bis(trifluoromethanesulfonyl)imide (Li-TFSI, 99%) were received from Acros Organics (Morris Plains, NJ, USA). Micro-90 cleaning solution and other chemicals were of analytical grade and obtained from Thermo Fisher Scientific Inc. (Pittsburgh, PA, USA).

2.2 Preparation of the silanized TiO_2/FTO substrate

FTO glass substrates were etched with a mixture of zinc powder and HCl solution (2 M), and cleaned in an ultrasonic bath successively with 1% micro-90 aqueous solution, deionized water, isopropanol, and acetone. A TiO_2 colloidal solution containing 0.26 M tetrabutyltitanate and 0.3 M ethanolamine was prepared with isopropanol. Upon casting 0.1 mL of this colloidal solution onto each FTO substrate (~1.8 × 1.5 cm), a compact TiO_2 layer was spin-coated at 500 rpm for 6 s and 3000 rpm for 30 s. The TiO_2/FTO substrates were annealed at 500 ^oC for 30 min and subsequently soaked in a toluene solution with [APS]/[MTMS] ratios of 100/0, 70/30, 50/50, 30/70, and 0/100. The resultant single or mixed organosilane monolayers were rinsed with toluene and dried under a nitrogen stream. The silanized TiO_2/FTO substrates were then laid out on a watch glass, which was placed in a large petri dish whose bottom was covered with deionized water. After the organosilane molecules had reacted with water vapor for at least 30 min, the substrates were baked at 125 ^oC for 1 h. Finally, these substrates were soaked in a 0.5% (w/w) HI solution for 1 min, which was followed by washing with deionized water and drying at 125 ^oC for 1 h.

2.3. Construction of Perovskite Solar Cells

About 0.1 mL of *N, N*-dimethylformamide containing 462 mg/mL PbI_2 was cast onto each silanized TiO_2/FTO substrate, which was subsequently spun at 4000 rpm for 40 s. Upon drying at 70 ^oC for 30 min, these substrates were soaked in an isopropanol solution containing 10 mg/mL CH_3NH_3I for 30 s. They were taken out from the solution and spun at 3000 rpm for 30 s to remove residual CH_3NH_3I. The perovskite/silanized TiO_2/FTO substrates were dried at 70 ^oC for another 30 min. Then the hole-transport material (HTM) was spin-coated on top of the surface at 2000 rpm for 30 s. The coating solution was prepared by dissolving 72.3 mg spiro-OMeTAD, 10 mg Li-TFSI, 10 mg Co-TFSI and 26.7 μL TBP in 1 mL chlorobenzene. Finally, a 90-nm-thick gold film was thermally evaporated as the topmost layer in vacuum. The overall assembly process described above was also performed in a glove box (Mbraun, Munich, Germany) circulated with dry N_2.

2.4. Surface Characterization

FT-IR spectra were collected with an FT-IR spectrometer (Thermo Nicolet 6700, Madison, WI, USA). X-ray diffraction (XRD) patterns were recorded with a D8 Advance X-ray diffractometer (Bruker, Madison, WI, USA) with Cu Kα radiation. Electrochemical experiments were conducted with a DY2300 potentiostat instrument (Digi-Ivy, Austin, TX, USA) in air with humidity around 40%. A 500 W Xe lamp (Newport Corp, Irvine, CA, USA) with an AM 1.5 filter was used as the simulated solar irradiation (100 mW/cm^2). The light intensity was measured with a radiant power meter (Model 70260, Newport Corp.). A black mask with an aperture of 0.08 cm^2, which defined the illuminated area and reduced the scattered light, was placed between the solar cells and the light source.

3. RESULTS AND DISCUSSION

Figure 1 shows schematically the use of mixed (panels a and c) and single (panel b) organosilane monolayers to template the perovskite film growth onto the TiO_2 layer. Using X-ray neutron diffraction, Christopher et al. measured the $CH_3NH_3PbI_3$ crystal lattice constant *a* (between two apical iodides) to be 6.28 Å [27]. This means that the distance between the two methylammonium ions in the perovskite crystal is also 6.28 Å. Thus, for the $-(CH_2)_3NH_3^+$ groups to serve as anchors to grow the bottommost layer of the perovskite film (i.e., mimicking methylammonium ions), the distance between two adjacent $(CH_2)_3NH_3^+$ groups (*l* in Figure 1a) should match this lattice constant. Based on the siloxane bond angle and length shown in Figure 1d [28, 29], for a mixed monolayer of 50/50 APS/MTMS, *l* can be calculated by the following equation:

$$l = 2b = 2d \times \sin(\theta/2) \quad (1)$$

where *b* the distance of two adjacent Si atoms, *d* the bond length of Si–O (1.64 Å), and θ the angle of the O–Si–O bond (142.5°). When a 50/50 mixed monolayer is formed, *l* corresponds to 6.21 Å, which is remarkably close to the lattice constant of 6.28 Å. With the iodide apexes of the perovskite crystal intercalate almost perfectly the $-(CH_2)_3NH_3^+$ anchor groups, the rest of the perovskite crystal can be

grown orderly from the surface with excellent crystallinity and orientation. In contrast, no cavities are available in the single APS monolayer for the intercalation of perovskite iodide ions. Consequently, distorted perovskite crystals are formed (Figure 1b). As for the mixed monolayer prepared with APS/MTMS compositions other than 50/50 (e.g. 70/30 as shown in Figure 1c), the mismatch between the spacing or cavities in the mixed monolayer and the perovskite lattice constant *a* also results in distorted or disordered perovskites.

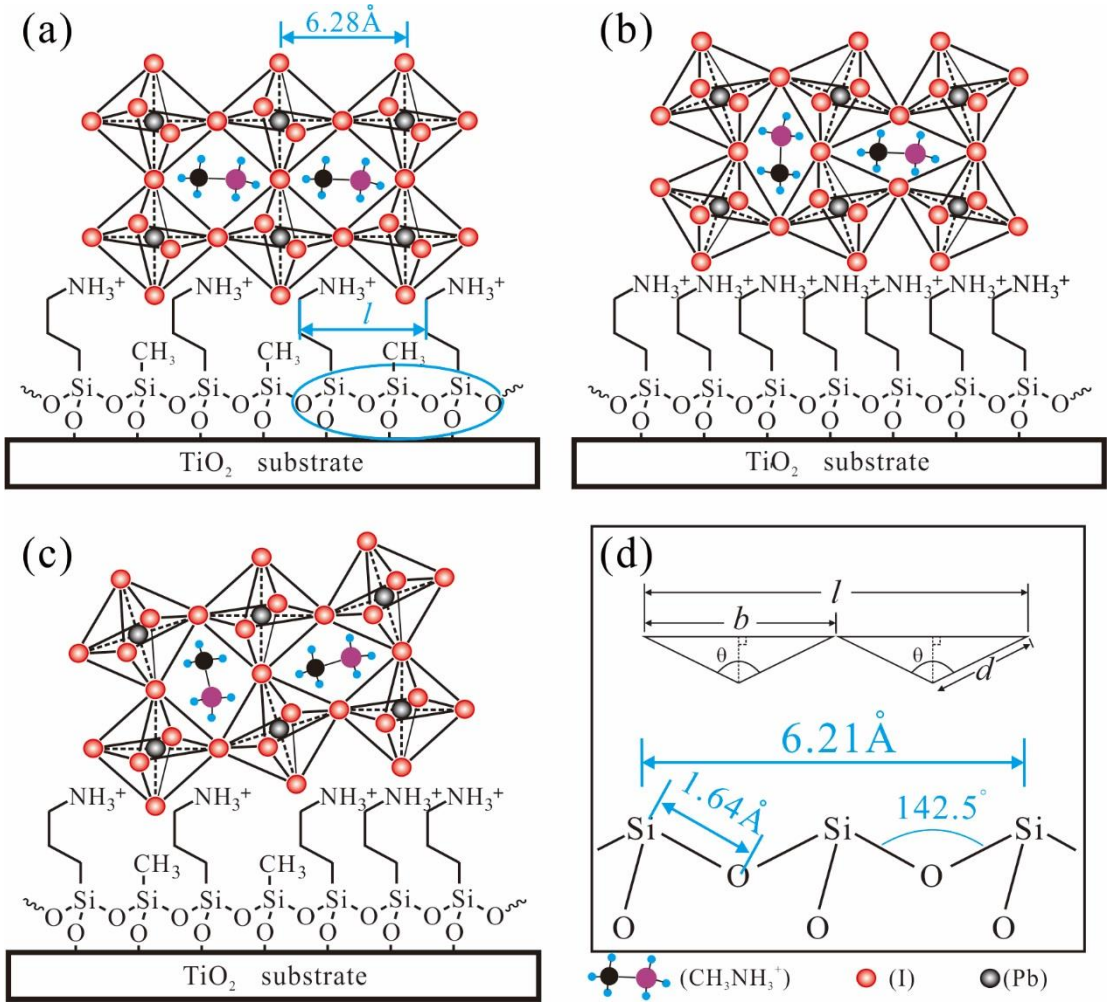

Figure 1. Schematic diagrams showing the use of the mixed (a and c) and single (b) organosilane monolayers to template perovskite growth on TiO_2. The mixed or single monolayers contained APS/MTMS compositions of (a) 50/50, (b) 100/0, and (c) 70/30. The red spheres represent iodide ions and the grey spheres denote lead ions. (d) The siloxane bond angle and length used to calculate the distance between two adjacent $-(CH_2)_3NH_3^+$ groups.

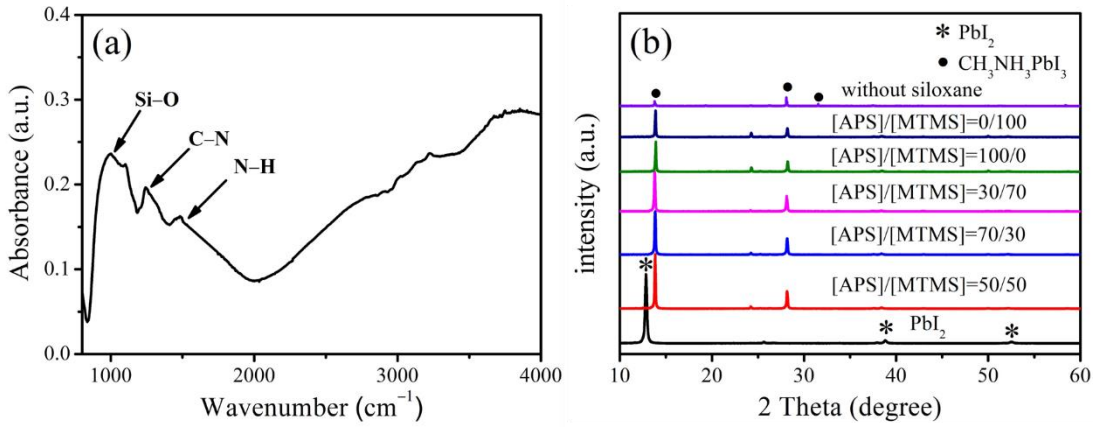

Figure 2. (a) An FT-IR spectrum of a TiO_2 film silanized in a solution containing [APS]/[MTMS] of 50/50. (b) XRD patterns of PbI_2, perovskite films grown directly on the TiO_2 layer, and perovskite films grown on single APS or MTMS monolayer and mixed monolayers of different APS/MTMS compositions.

To confirm our geometric calculation and prediction, we prepared mixed APS/MTMS monolayers in different compositions for subsequent perovskite film growth. Successful formation of the mixed monolayers was confirmed by FT-IR spectroscopy (Figure 2a). The two bands at 1240 cm^{-1} and 1500 cm^{-1} can be assigned to the C–N stretching and N–H bending modes, respectively. In addition, the peak at 1000 cm^{-1} is characteristic of the Si–O–Si stretching in the siloxane layer [13, 30]. These results indicate that a siloxane layer has been formed at the hydroxylated TiO_2 surface [31, 32]. We also employed X-ray diffraction (XRD) to probe the crystallinity and orientation of the perovskite films. Figure 2b shows the XRD patterns of perovskite films grown on mixed monolayers of APS/MTMS in different compositions. For comparison, the XRD pattern of PbI_2 was also recorded (Figure 2b), in which the strong diffraction peak at 12.7° corresponds to the (001) plane of PbI_2 [33]. When PbI_2 reacts with CH_3NH_3I to form the $CH_3NH_3PbI_3$ perovskite, this diffraction peak is completely replaced by those of $CH_3NH_3PbI_3$. The diffraction pattern of the perovskite film directly grown onto the TiO_2 compact layer (i.e. without silinization) shows three weak peaks at 13.8°, 28.1°, and 31.5°, which are respectively assigned to the (110), (220), and (312) planes of the $CH_3NH_3PbI_3$ perovskite crystal [34]. This result implies that the perovskite layer has low crystallinity and low crystal orientation. In contrast, stronger diffractions were observed for the perovskite films formed at mixed monolayers containing different APS/MTMS compositions, with the (110) and (220) diffraction peaks being the strongest for the perovskite grown onto a mixed monolayer of 50/50 APS/MTMS. These XRD results suggest that the perovskite crystals preferentially grown along the directions of (110) and (220) facets, and the crystallinity and orientation can be modulated by using different [APS]/[MTMS] ratios in solution. It is evident that the evenly spaced Si–O–$(CH_2)_3NH_3^+$ and SiO–CH_3 groups served as the template to guide the subsequent growth of the perovskite. The excellent agreement between the perovskite lattice constant and our calculated spacing also indicates that our surface modification procedure affords precise control of the compositions of the mixed monolayers.

.

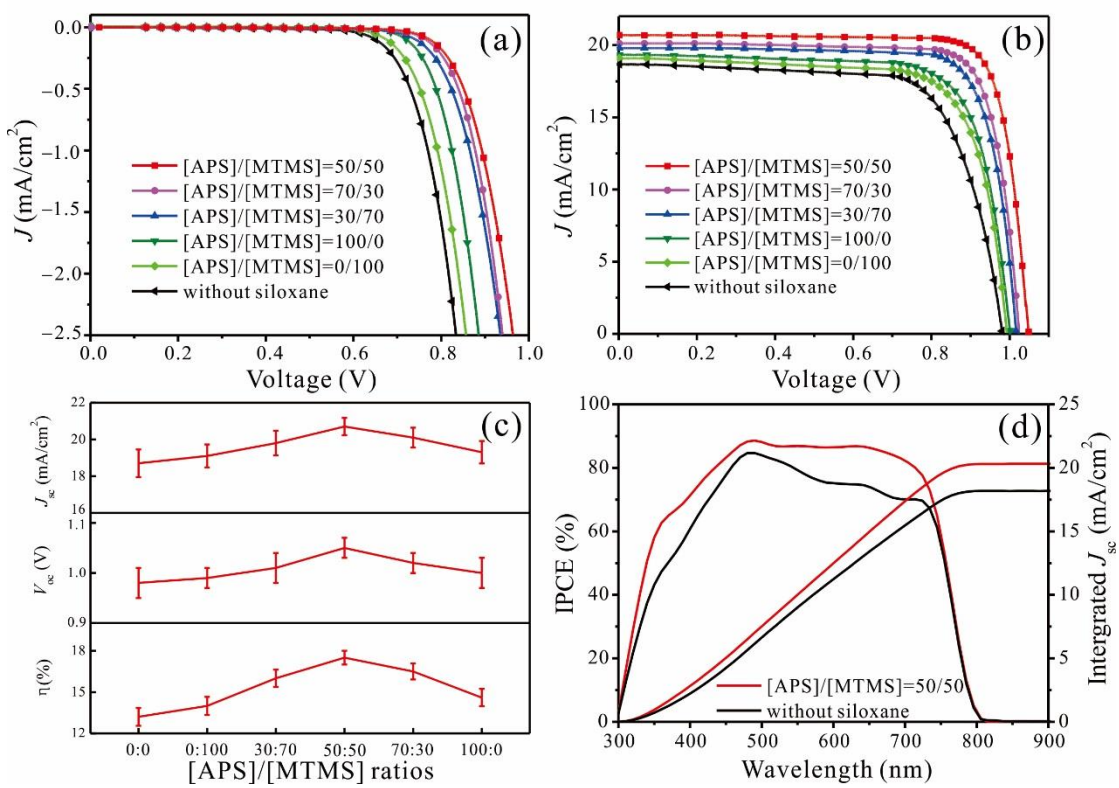

Figure 3. *J–V* curves recorded in dark (a) and under 100 mW/cm^2 illumination (b) of a PSC constructed with a perovskite film grown without a monolayer and PSCs constructed with perovskite films grown on single APS or MTMS monolayers or mixed monolayers of different APS/MTMS compositions. (c) Impact of the APS/MTMS composition on the performance of PSCs. More than 10 PSCs were assembled for each APS/MTMS composition ratios and the curves were all recorded in air. (d) IPCE spectra of the devices without siloxane and with a mixed monolayer of APS/MTMS (50/50).

Perovskites with higher crystallinity contain less defects, hence the photohole/electron recombination rate is retarded. However, lattice orientation of a highly ordered perovskite film can also affect the photovoltaic performance due to possible anisotropic charge mobility along different crystal planes. Only when the charge mobility is enhanced along the (110) lattice plane or remains as high as those along other planes [15, 35], can highly oriented perovskite films lead to better photovoltaic performance. To confirm that the strong (110) diffraction peak is indeed an indication of high charge mobility, we investigated how the APS/MTMS compositions in the mixed monolayers affect the photovoltaic performance of the PSCs. Figure 3a and 3b show the PSC performance in dark and under illumination, respectively. In dark, the PSC constructed with perovskite films grown onto single or mixed siloxane monolayers all exhibit smaller currents than that grown directly onto a bare TiO_2 surface (i.e. no silanization). This suggests that the siloxane layer helps block undesired charge transport across the interface. In addition, the difference in the dark currents among PSCs with perovskite films grown onto different mixed monolayers indicates that the number of defects is dependent on the quality of the perovskite film. The film grown on top of the monolayer of 50/50 APS/MTMS produced the lowest dark current or the least number of defects [36]. Under illumination of 100 mW/cm^2 (Figure 3b), the PSC

with a perovskite film grown directly onto bare TiO_2 produced J_{SC} of only 18.7 mA/cm^2 and V_{OC} of only 0.98 V. In contrast, with a mixed monolayer of the optimal APS/MTMS ratio, significantly higher J_{SC} (20.7 mA/cm^2) and V_{OC} (1.05 V) values were obtained. Apparently, a hydrophobic monolayer is more compatible with the methylammonium lead halide perovskite. Our observation is consistent with previous reports on that a siloxane layer between TiO_2 and perovskite is beneficial for enhancing the electron transport and suppressing the hole/electron recombination [13, 15, 19, 34]. Clearly, these results suggest that the perovskite orientation and lattice match the spacing between the $–(CH_2)_3NH_3^+$ anchors. In addition to the decreased charge recombination, the augmented fill factor (*FF*) is indicative of a gradual decrease in the internal resistance of the PSC (Figure 3c) [37]. The integrated current densities from the incident photon-to-electron conversion efficiency (IPCE) curve were 18.2 and 20.3 mA/cm^2 for the two devices without siloxane and with a mixed monolayer of the optimal APS/MTMS ratio, which are almost in agreement with the measurements in this study (Figure 3d). Therefore, the APS/MTMS (50/50) treatment significantly improved the performance of PSCs through more efficient electron collection [19]. In addition, the absorption threshold is 1.55 eV, which is consisitent with the bandgap of $CH_3NH_3PbI_3$ [1, 8, 9]. In Table 1 we summarized the photovoltaic parameters of various PSCs reported in recent years, along with those of our PSCs assembled and tested under different conditions. Evidently the efficiency of our PSC assembled in inert atmosphere and tested in air compares well to those of PSCs assembled and tested both in inert atmosphere [38] and favorably to those without assembling and testing conditions specified [14, 15, 34]. Notice that there is still a little gap between the efficiency of our PSC and the best batteries reported [39-42]. This is not surprising as it is well known organic lead halide perovskite-based solar cells, without special treatments, have chemical and photochemical instabilities in air [1, 8, 39-42]. As can be seen from other reports listed in Table 1, doping $CH_3NH_3PbI_3$ with chloride ions [8] and thiocyanate ($SCN^–$) [41] and treating water-containing $CH_3NH_3PbI_3$ with dimethylformamide (DMF) resulted in higher chemical stability [42], while the phenethylammonium iodide (PEAI)-modified perovskite film appeared to have suppressed non-radiative recombination, hence enhanced photochemical stability [40].

Table 1. Comparison of Performance of Various PSCs

PSC Structures	Preparative/Test Conditions	V_{OC} (V)	J_{SC} (mA/cm^2)	*FF* (%)	η (%)	Ref.
FTO/TiO_2/mixed SAM/$CH_3NH_3PbI_3$/spiro-OMeTAD/Au	in inert atmosphere /in air	1.05	20.70	80	17.52	this work
FTO/TiO_2/SAM/ZrO_2^+ $CH_3NH_3PbI_3$/carbon	N/A	0.87	19.50	75	12.77	14
FTO/TiO_2/HOCO–R–$NH_3^+I^–$ $CH_3NH_3PbI_3$/spiro-OMeTAD/Ag^+Au	N/A	1.00	19.20	62	12.00	15
FTO/TiO_2/$CH_3NH_3PbI_3$/SAM/ spiro-OMeTAD/Ag	N/A	0.90	16.55	72	11.80	34

ITO/PEDOT:PSS/ polyTPD/$CH_3NH_3PbI_3$/Au	Both in inert atmosphere	1.09	18.2	75	14.80	38
ITO/Yttrium-doped TiO_2/$CH_3NH_3PbI_{3-x}$ Cl_x/spiro-OMeTAD/Au	Both in air	1.13	22.75	75	19.30	8
ITO/SnO_2/FA_{1-x} $(CH_3NH_2)_xPbI_3$/PEAI/spiro-OMeTAD/Au	Both in air	1.18	25.20	78	23.32	40
FTO/TiO_2/mesoporous-TiO_2/ $CH_3NH_3PbI_{3-x}(SCN)_x$/spiro-OMeTAD/Au	Both in air	0.96	20.90	72	14.52	41
ITO/PEDOT:PSS/ $CH_3NH_3PbI_3$-X/Ca/Al	Both in air	1.03	23.51	83	20.10	42

SAM: self-assembled monolayer; ITO: indium tin oxide; FA: $HC(NH_2)_2$; polyTPD: poly(4-butylphenyl-diphenyl-amine); PEAI: phenethylammonium iodide; PEDOT:PSS: poly (3,4-ethylenedioxythiophene):poly(styrenesulfonate); $CH_3NH_3PbI_3$-X: $CH_3NH_3PbI_3$ films containing different (X) water contents and treated with DMF. N/A: not available.

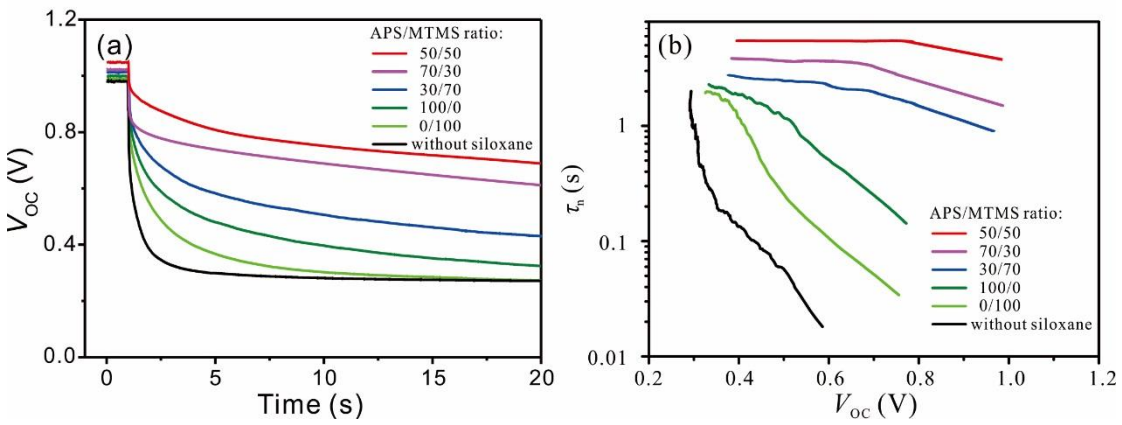

Figure 4. (a) Open-circuit voltage decays and (b) electron lifetimes in PSCs constructed with TiO_2 layers without siloxane (black) and with single APS or MTMS monolayers or mixed monolayers of different APS and MTMS compositions (in colors).

As described above, the interdigitated $-(CH_2)_3NH_3^+$ anchors link the compact TiO_2 layer and the perovskite film to facilitate charge transport, while the siloxane layer at the bottom acts as an energy barrier for blocking the photohole/electron recombination [43]. The electron lifetime (τ_n) in PSCs has been considered as a parameter for gauging the presence of charge recombination sites and the magnitude of the recombination kinetics. Traditionally, upon taking into account the thermal energy, the derivatives of the V_{OC} decay curves are an indirect way of measuring τ_n [44].

$$\tau_n = -\frac{k_B T}{e}\left(\frac{dV_{oc}}{dt}\right)^{-1} \quad (2)$$

where k_B is the Boltzmann constant, T the absolute temperature, e the electronic charge, and dV_{OC}/dt the derivative of the transient V_{OC}. As shown in Figure 4a, V_{OC} decayed with time right after termination of irradiation, indicating that the photogenerated electrons had moved across the interfaces between the

TiO_2 layer, the siloxane layer, and the perovskite film to recombine with holes. For a simple one-step recombination, an exponential decay V_{OC} is observable, which is linearly correlated to the charge lifetime [13]. It is apparent in Figure 4b that the electron lifetime in the PSC with the perovskite film grown directly on bare TiO_2 is the shortest and has no linear dependence on V_{OC}. Such a phenomenon is indicative of the presence of multiple recombination mechanisms (steps). We think that this is most likely caused by TiO_2 channels or sites that are in direct contact with the HTM layer (due to a patchy perovskite film) and the defects in the disordered perovskite film. In contrast, τ_n significantly increased in PSCs constructed with perovskite films grown on top of mixed monolayers. This indirectly confirmed that the underlying mixed organosilane monolayer can block the fastest recombination channels, including sites or pinholes in the perovskite film that otherwise leads to shorting between the TiO_2 and HTM layers. As the recombination rate decreases, the electron lifetime increases. Although our optimal PSC possessed the longest electron lifetime, the V_{OC} dependence of the electron lifetime exhibited multiple slopes, which are indicative of multiple recombination routes. Particularly, in the high V_{OC} regime there are fast recombination routes. In general, the trend exhibited by different PSCs is in line with the *J–V* curves (cf. Figure 3b). All these characteristics demonstrate that the $-(CH_2)_3NH_3^+$ groups in the mixed monolayer have served as anchors and become part of the bottommost layer of the perovskite film. On the basis of the enhance conversion efficiency, utilizing a perovskite whose lattice orientation is perpendicular to the electrode surface to facilitate charge transportation is more effective than blocking charge recombination with a monolayer of one compound [14, 15, 22, 45]. The presence of multiple charge-recombination routes in our PSCs, however, suggests that defects still exist in the perovskite film produced even with the optimal APS/MTMS ratio. Thus, future attention should be paid to developments of more suitable substrates (e.g. a smoother TiO_2 compact layer), surface modification methods (doping of the TiO_2 layer and the perovskite film), chemical and photochemical treatments of the perovskites to afford a PSC efficiency that is closer the theoretical prediction (31% [46]).

4. CONCLUSIONS

We devised a new strategy for constructing methylammonium lead iodide perovskite solar cell by controllably growing the perovskite film onto a template of mixed APS/MTMS monolayer. The protruding $-(CH_2)_3NH_3^+$ groups of the mixed monolayer, which is covalently attached to a compact TiO_2 layer, minimizes the steric hindrance for the formation of highly ordered methylammonium lead iodide perovskite. The calculated spacing between these anchors indicates that a surface coverage of 50% of APS matches the lattice constant of the perovskite crystal. XRD characterization confirmed that the mixed monolayer facilitated the orientational growth of the (110) and (220) phases at the interface. Corresponding to the highest order of orientationally grown perovskite film, the PSC constructed in an inert atmosphere yielded good photovoltaic performance that compares well with other reported methylammonium lead iodide-based PSCs. The high performance is attributable to the facile charge transportation in the ordered perovskite film. The long electron lifetime suggests that at the interfaces and within the bulk perovskite film the defects and charge recombination sites are limited. This proof-

of-concept approach demonstrates that judicious designs and modifications of interfaces in solar cells can help enhance photovoltaic performance.

ACKNOWLEDGMENTS
This work was partially supported by the NSF-CREST Program at California State University, Los Angeles (NSF No. HRD-1547723), the Natural Science Foundation of China (No. 21802051), and the Natural Science Foundation of Shandong Province, China (No. ZR2019QB007).

NOTES
The authors declare no competing financial interest.

References

1. M. Grätzel, *Nat. Mater.*, 13 (2014) 838.
2. Z.G. Xiao, Q.F. Dong, C. Bi, Y.C. Shao, Y.B. Yuan and J.S. Huang, *Adv. Mater.*, 26 (2014) 6503.
3. H.S. Kim, C.R. Lee, J.H. Im, K. B. Lee, T. Moehl, A. Marchioro, S.J. Moon, R. Humphry-Baker, J.H. Yum, J.E. Moser, M. Gratzel and N.G. Park, *Sci. Rep.*, 2 (2012) 591.
4. Y. Kumar, E. Regalado-Pérez, A. M. Ayala, N. R. Mathews and X. Mathew, *Sol. Energ. Mat. Sol. C.*, 157 (2016) 10.
5. G.C. Xing, N. Mathews, S.Y. Sun, S.S. Lim, Y.M. Lam, M. Gratzel, S. Mhaisalkar and T.C. Sum, *Science*, 342 (2013) 344.
6. Q.F. Dong, Y.J. Fang, Y.C. Shao, P. Mulligan, J. Qiu, L. Cao and J.S. Huang, *Science*, 347 (2015) 967.
7. C. Wehrenfennig, G.E. Eperon, M.B. Johnston, H.J. Snaith and L.M. Herz, *Adv. Mater.*, 26 (2014) 1584.
8. H.P. Zhou, Q. Chen, G. Li, S. Luo, T.B. Song, H.S. Duan, Z.R. Hong, J.B. You, Y.S. Liu and Y. Yang, *Science*, 345 (2014) 542.
9. Y.C. Shao, Y.B. Yuan and J.S. Huang, *Nat. Energy*, 1 (2016) 15001.
10. Best Research-Cell Efficiency Chart, https://www.nrel.gov/pv/cell-efficiency.html (2019).
11. A. Hagfeldt, G. Boschloo, L. Sun, L. Kloo and H. Pettersson, *Chem. Rev.*, 110 (2010) 6595.
12. A. Burke, S. Ito, H. Snaith, U. Bach, J. Kwiatkowski and M. Grätzel, *Nano. Lett.*, 8 (2008) 977.
13. D.L. Jiang, Y.Q. Hao, R.J. Shen, S. Ghazarian, A. Ramos and F.M. Zhou, *ACS Appl. Mater. Inter.*, 5 (2013) 11906.
14. L.F. Liu, A.Y. Mei, T.F. Liu, P.Jiang, Y.S. Sheng, L.J. Zhang and H.W. Han, *J. Am. Chem. Soc.*, 137 (2015) 1790.
15. Y. Ogomi, A. Morita, S. Tsukamoto, T. Saitho, Q.Shen, T. Toyoda, K. Yoshino, S.S. Pandey, T.L. Ma and S. Hayase, *J. Phys. Chem. C*, 118 (2014) 16651.
16. Y.C. Shih, L.Y. Wang, H.C. Hsieh and K.F. Lin, *J. Mater. Chem. A*, 3 (2015) 9133.
17. L.J. Zuo, Z.W. Gu, T. Ye, W.F. Fu, G. Wu, H.Y. Li and H.Z.Chen, *J. Am. Chem. Soc.*, 137 (2015) 2674.
18. L. Zhang, X. Liu, J. Li and S. Mckechnie, *Sol. Energ. Mat. Sol. C.*, 175 (2018), 1.
19. Y.Q. Wang, S.B. Xu, J.G. Deng and L.Z. Gao, *Roy. Soc. Open Sci.*, 4 (2017) 170980.
20. Z.H. Liu, Q. Chen, Z.R. Hong, H.P. Zhou, X.B. Xu, N. De Marco, P.Y. Sun, Z.X. Zhao, Y. B. Cheng and Y. Yang, *ACS Appl. Mater. Inter.*, 8 (2016) 11076.
21. J. Cao, J. Yin, S.F. Yuan, Y. Zhao, J. Li and N.F. Zheng, *Nanoscale*, 7 (2015) 9443.
22. A. Mingorance, H.B. Xie, H.S. Kim, Z.W. Wang, M. Balsells, A. Morales-Melgares, N. Domingo, N. Kazuteru, W. Tress, J. Fraxedas, N. Vlachopoulos, A. Hagfeldt and M. Lira-Cantu, *Adv. Mater. Interfaces*, 5 (2018) 1800367.

23. J.J. Gooding and S. Ciampi, *Chem. Soc. Rev.*, 40 (2011) 2704.
24. J. Lahiri, L. Isaacs, J. Tien and G.M. Whitesides, *Anal. Chem.*, 71 (1999) 777.
25. G.B. Sigal, C. Bamdad, A. Barberis, J. Strominger and G.M. Whitesides, *Anal. Chem.*, 68 (1996) 490.
26. C. Pale-Grosdemange, E.S. Simon, K.L. Prime and G.M. Whitesides, *J. Am. Chem. Soc.*, 113 (1991) 12.
27. C. Eames, J.M. Frost, P.R.F. Barnes, B.C. O'Regan, A. Walsh and M.S. Islam, *Nat. Commun.*, 6 (2015) 7497.
28. A.N. Parikh, D.L. Allara, I.B. Azouz and F. Rondelez, *J. Phys. Chem.*, 98 (1994) 7577.
29. H. Steinfink, B. Post and I. Fankuchen, *Acta Crystallogr.*, 8 (1955) 420.
30. S.M. Feldt, U.B. Cappel, E.M.J. Johansson, G. Boschloo and A. Hagfeldt, *J. Phys. Chem. C*, 114 (2010) 10551.
31. J. Wang, S. Zheng, Y. Shao, J. Liu, Z. Xu and D. Zhu, *J.Colloid Interf. Sci.*, 349 (2010) 293.
32. H. Sardon, L. Irusta, M.J. Fernández-Berridi, M. Lansalot and E. Bourgeat-Lami, *Polymer*, 51 (2010) 5051.
33. Y.Z. Wu, A. Islam, X.D. Yang, C.J. Qin, J. Liu, K. Zhang, W.Q. Peng and L.Y. Han, *Energ. Environ. Sci.*, 7 (2014) 2934.
34. J. Zhang, P. Wang, X.K. Huang, J. Xu, L.M. Wang, G.Q. Yue, X.W. Lu, J.W. Liu, Z.Y. Hu, Q. Wang and Y.J. Zhu, *RSC Adv.*, 6 (2016) 9090.
35. Z. Wu, S. Bai, J. Xiang, Z. Yuan, Y. Yang, W. Cui, X. Gao, Z. Liu, Y. Jin and B. Sun, *Nanoscale*, 6 (2014) 10505.
36. N.J. Jeon, J. Lee, J.H. Noh, M.K. Nazeeruddin, M. Grätzel and S.I. Seok, *J.Am. Chem. Soc.*, 135 (2013) 19087.
37. Z. Zekry and G. Eldallal, *Solid-State Electron.*, 31 (1988) 91.
38. O. Malinkiewicz, C. Roldán-Carmona, A. Soriano, E. Bandiello, L. Camacho, M. K. Nazeeruddin and H.J. Bolink, *Adv. Energy Mater.*, 4 (2014) 1400345.
39. Y. Zhang, M. Rong, X. Yan, X. Wang, Y. Chen, X. Li and R. Zhu, *Langmuir*, 34 (2018) 9507.
40. Q. Jiang, Y. Zhao, X. Zhang, X. Yang, Y. Chen, Z. Chu, Q. Ye, X. Li, Z. Yin and J. You, *Nat. Photonics*, 13 (2019) 460.
41. Q. Tai, P. You, H. Sang, Z. Liu, C. Hu, H.L.W. Chan and F. Yan, *Nat. Commun.*, 7 (2016) 11105.
42. C.H. Chiang, M.K. Nazeeruddin, M. Grätzel and C.G. Wu, *Energ. Environ. Sci.*, 10 (2017) 808.
43. J. Zhang, Z.L. Hu, L.K. Huang, G.Q. Yue, J.W. Liu, X.W. Lu, Z.Y. Hu, M.H. Shang, L.Y. Han and Y.J. Zhu, *Chem. Commun.*, 51 (2015) 7047.
44. J. Bisquert, F. Fabregatsantiago, I. Moraseró, G. Garciabelmonte and S. Giménez, *J. Phys. Chem. C*, 113 (2009) 17278.
45. W.Y. Nie, H.H. Tsai, J.C. Blancon, F.Z. Liu, C.C. Stoumpos, B. Traore, M. Kepenekian, O. Durand, C. Katan, S. Tretiak, J. Crochet, P.M. Ajayan, M.G. Kanatzidis, J. Even and A.D. Mohite, *Adv. Mater.*, 30 (2018) 1703879.
46. S. Rühle, *Sol. Energy*, 130 (2016) 139.